iScience

Article

Common developmental origins of beak shapes and evolution in theropods

Graphical abstract

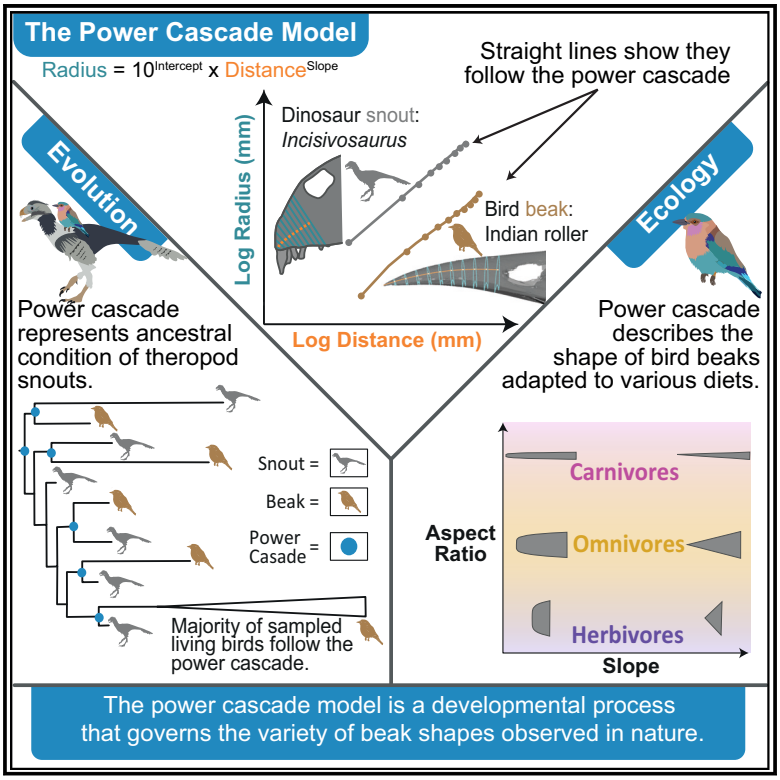

Highlights

- The power cascade is a conserved growth model for theropod beak and snout shape
- The power cascade generates the primordial shape of the vertebrate rostrum
- Beaks of most species follow the power cascade to fill many adaptive functions
- The power cascade has shaped the face of theropods for 200 million years

Authors

Kathleen L.S. Garland, Eleanor M. Hay, Daniel J. Field, Alistair R. Evans

Correspondence

kathleen.garland@monash.edu (K.L.S.G.), alistair.evans@monash.edu (A.R.E.)

In brief

Ornithology; Evolutionary biology; Phylogeny; Animal morphology

Garland et al., 2025, iScience 28, 112246
April 18, 2025
https://doi.org/10.1016/j.isci.2025.112246

CellPress

iScience

CellPress
OPEN ACCESS

Article

Common developmental origins of beak shapes and evolution in theropods

Kathleen L.S. Garland,[1,5,*] Eleanor M. Hay,[1,2] Daniel J. Field,[3] and Alistair R. Evans[1,4,*]
[1]School of Biological Sciences, Monash University, Melbourne, VIC, Australia
[2]Department of Biology, University of Miami, Coral Gables, FL 33146, USA
[3]Department of Earth Sciences & Museum of Zoology, University of Cambridge, Cambridge, UK
[4]Museums Victoria Research Institute, Museums Victoria, Melbourne, VIC, Australia
[5]Lead contact
*Correspondence: kathleen.garland@monash.edu (K.L.S.G.), alistair.evans@monash.edu (A.R.E.)
https://doi.org/10.1016/j.isci.2025.112246

SUMMARY

Vertebrate beaks show a remarkable diversity of forms, epitomized by birds and non-avian theropods. Few studies have investigated how underlying developmental processes influence beak shape. The power cascade is a model of growth describing the log-log linear relationship of the beak radius with distance from the tip. We measured beak and toothed snout shapes in 127 species across 120 families of extant birds and extinct non-avian theropods and found that 95% followed the power cascade model. Ancestral state estimation suggests that the power cascade constitutes a fundamental growth pattern of the theropod rostrum, and perhaps all vertebrate rostra. The morphospace defined by the power cascade shows how bird beak shape explores the geometries associated with ecological specializations while adhering to the growth model. We show that the power cascade influences the macroevolutionary exploration of rostrum morphospace, enabling extant birds to inhabit all components of Earth's biosphere.

INTRODUCTION

Universal models of growth are rare but highly beneficial to the field of evolutionary developmental biology.[1–3] These models are advantageous as they can be applied across large evolutionary and developmental scales.[4] In spanning multiple levels, models of growth reveal how development and evolution interact to influence the morphological diversity we observe in nature.

The logarithmic spiral has long been recognized as a universal model of biological growth. First observed in shells,[5] then teeth, horns, and claws,[1] the logarithmic spiral is formed when one side of a structure grows faster than the other at a constant rate and angle relative to the origin of the spiral. The logarithmic spiral has been observed from the cellular to morphological level.[6] As a component of shape independent of the logarithmic spiral, the power cascade growth model generates biological pointed and spiral shapes. The power cascade is a power law that describes the change in the width of a structure as it lengthens from tip to base.[7] The parameters of the power cascade describe the shape of a structure, where the *Aspect Ratio* is how relatively long a pointed structure is and the *Slope* is how conical to blunt the structure is. Over 200 pointed and spiral structures across the animal kingdom adhere to the power cascade model, including mammal teeth and claws, ungulate hoof bones, fish spines, plant thorns, gastropod shells, and bird and non-avian dinosaur bony beaks.[7]

Toothless beaks have evolved multiple times in theropod evolution and are, therefore, a promising structure to consider when exploring the universality of the power cascade model. Indeed, beaks have evolved at least six times throughout theropod evolution.[8,9] Similar to previous definitions, a beak here is defined as an elongated premaxilla that is toothless.[8–11] Each theropod beak has evolved from a toothed rostrum comprising both maxilla and premaxilla bone, herein referred to as a 'snout'.[11] Extensive fossil beak descriptions (e.g., *Khaan*,[12] *Confuciusornis*,[13] *Falcatakely*,[14] and *Jeholornis*[15]) have helped in understanding the range of rostral shapes and foraging behaviors of extinct theropods. The causes of the independent instances of theropod beak evolution are suspected to be lineage-specific,[9] and include ecological factors like diet (herbivory and granivory[12,16,17]). However, the repeated evolution of the beak may also be related to developmental factors,[9,18–20] such as reduced incubation periods and transitions toward pedomorphy and peramorphy.[18,21–23] This convergent evolution of theropod beaks may be indicative of developmental processes described by a rule of growth, such as the power cascade model.

Across avian evolution, bird beak and cranial morphology have been found to relate to functional and ecological adaptations.[24–28] However, due to suspected underlying evolutionary and developmental constraints, fine-scale correlations between beak shape and behavior are difficult to detect.[21,24,25,27,29,30] Previous work has formulated a growth model to describe the beak shape in a restricted group of passerines.[31–37] However, no study has sought to investigate how models of growth may apply to a broader range of beak diversity. The power cascade may be a universal rule of growth that describes the evolution of bird beaks and, more broadly, vertebrate beaks.

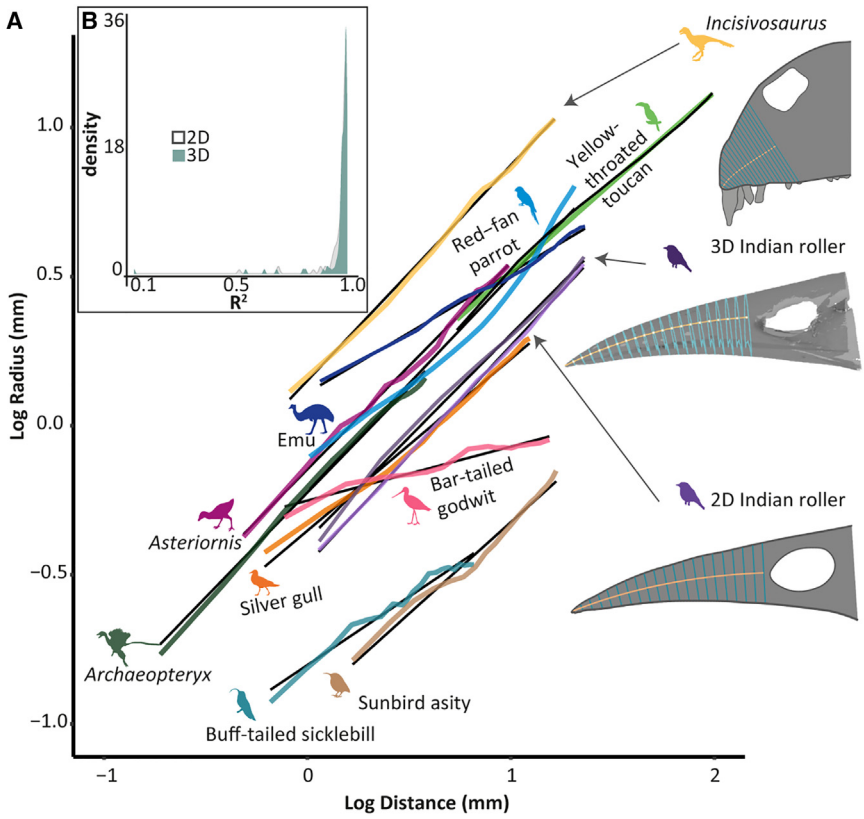

Figure 1. The rostra (beak and snout) of many theropods grows according to the power cascade model

(A) The linear relationship between *Log Radius* with *Log Distance (mm)* for the premaxilla rostral to the nares. Plots for Indian roller measured in 2D (R^2 = 0.999) and 3D (R^2 = 0.996) show that both types of measurement capture the power cascade.

(B) Histogram of adjusted R^2 values for fit to the power cascade linear model measured in 3D and 2D, including measurements of all beak elements (tip, prenarial, and whole) in simple and compound beaks. For Phylopic silhouettes attributions, refer to the key resources table. Other silhouettes were drawn by K.L.S.G. Indian Roller (NHMUK_S1987) 3D model from TempoBird Project – Morphosource. Incisivosaurus snout outline from Balanoff et al. (2009). American Museum Novitates.

This study aims to test the influence of the power cascade model on the evolution of theropod beak shape. We hypothesize that convergently evolved theropod beaks follow this growth model if the power cascade is a shared developmental pattern. We also aim to test how selective ecological factors, including diet, foraging niche, and habitat, influence the degree to which extant bird beak morphologies follow the power cascade model. We expect that bird beak shapes will follow the power cascade pattern of growth and evolve diverse beak morphological adaptations that are specialized for various ecological factors.

RESULTS

The power cascade captures the growth and morphology of beaks in 3D and 2D

The power cascade model describes the growth of the upper beak (bony premaxilla) as it expands laterally from the tip to the base (Figure 1A; Figure S1). We made 3D and lateral-view 2D measurements of 106 extant bird beaks spanning the avian phylogeny (106 out of 253 families and 42 out of 44 orders, Table S1). To test the power cascade, we fit a linear model to the radius and distance measurements for 20 equally spaced cross-sections perpendicular to the midline along the beak (Figure 1A). We concluded that the beak shape fit the power cascade when the R^2 of the linear model was greater than 0.90. To ensure comparability among beak types, we focused on the prenarial (the premaxilla rostral to the nares) region of the beak (Figure S2). 99 out of 106 (93.4%) extant bird beaks followed the power cascade model ($0.911 \leq R^2 \leq 0.999$; $p < 0.0001$; Figure 1B; Table S2) when measured in 3D. In 2D, 100 of the 106 extant birds (94.33%) had beaks that followed the power cascade model ($0.906 \leq R^2 \leq 0.999$; $p < 0.0001$; Figure 1B; Table S3).

The power cascade model parameters were very similar whether measured in 2D or 3D, with significant correlations for *Slope and Intercept* ($p < 0.001$; adjusted $R^2 < 0.70$; Figure S3; Table S3).

The power cascade is a conserved pattern of growth for the theropod premaxilla

By measuring the power cascade model in 2D, we were able to investigate if the growth model explains independent instances of theropod beak shape evolution. In addition to the extant birds, we measured 21 extinct theropod rostra in 2D, with teeth present or absent (i.e., beaks and snouts), following the power cascade model of growth (Figures 1A; Table S1, $n = 127$). For the purpose of our study, we considered a rostrum to be a 'beak' when the premaxilla was toothless, while toothed premaxillae were defined as 'snouts'. All 2D non-avian theropod taxa had prenarial premaxilla (beak and snouts) that significantly followed the power cascade model of growth ($0.927 \leq R^2 \leq 0.999$; $n = 21$; Figure S4).

To find when snouts or beaks first followed the power cascade and see whether the power cascade independently evolved in beaks across theropods, we studied the evolutionary patterns of the R^2 value. We consider that R^2, while not the standard phenotypical data used for these methods, is still appropriate for these analyses. This is because we consider that the R^2 is a measure of shape, specifically the degree to which the beak follows the power cascade. After comparing against unbounded Brownian and Ornstein-Uhlenbeck (OU) models of evolution, we found a bounded Brownian motion model (BBM[38]) to best fit the evolution of the R^2 values for all theropods (Table S4).

We then mapped the ancestral state estimates of the R^2 BBM on the composite time-scaled phylogeny. The ancestral state estimated for all theropod taxa premaxillary shapes followed the power cascade growth model (R^2 = 0.986, Figure S5). Across the non-avian theropod phylogeny from the root of Maniraptoriforms, the modeled evolution of the estimated R^2 value was always equal to or greater than 0.90. All nodes in the tree were >0.90.

We also explored how the rate of evolution of the R^2 value changed over theropod evolution using a continuous relaxed Brownian motion model implemented in RevBayes.[39] The rate of R^2 evolution decreased over time across the theropod phylogeny (Figure S6). There was a decrease in the rates with the evolution of crown birds. The fastest evolution rates occurred before the end of the Cretaceous (~100 mya). A subsequent slowdown in rates was observed in the clades of crown birds: (1) Psittacopasseres, (2) Coraciimorphae and Accipitrimorphae, (3) Phaethoquornithes, (4) Charadriiformes, Gruiformes, Strisores, Galliformes, Anseriformes, and Palaeognathae.

The power cascade parameters can describe the evolution of theropod snout and beak shape

When mapping the *Slope* and *Log Aspect Ratio* parameters onto the theropod phylogeny, we find that after the evolution of crown birds (late Cretaceous ~65 mya), the diversity of power cascade beak shapes was markedly greater than the ancestral theropod taxa (Figures 2A and 2C).

We explored this power cascade shape diversity by plotting the two parameters, *Slope* and *Log Aspect Ratio,* in a morphospace for those taxa that followed the power cascade ($R^2 \geq$ 0.90, Figure 2B). The *Log Aspect Ratio* describes how relatively gracile the premaxilla shape is, where larger aspect ratio values are thinner. The theropod with the shortest-shaped beak is *Jeholornis curvipes*, while the Eurasian hoopoe (*Upupa epops)* has the most gracile beak shape (Figure 2B). Along the *Log Aspect Ratio* axis, non-avian theropods occupy the bottom half of the morphospace and have squat rostral shapes (Figure 2B). Both extinct and extant Avialae cover a wider range of *Log Aspect Ratio* values. However, unlike the extinct avialans, the extant birds covered a greater range of *Log Aspect Ratio* values, showing the most gracile or narrow beaks in the morphospace.

The *Slope* value describes how conical/triangular to blunt the beak shape is. In 2D, a *Slope* value of 1 is an isosceles triangle, and less than 1 describes a progressively blunter beak (with a parabola shape at 0.5). The Eastern osprey (*Pandion cristatus*), razor-billed curassow *(Mitu tuberosum)*, and helmeted guineafowl (*Numida meleagris*) had *Slope* values greater than 1, indicating they are convex and pointed in shape at the tip. The bar-tailed godwit (*Limosa lapponica*) had the lowest *Slope* value and the bluntest beak tip shape. *Slope* values are more restricted in extinct Avialae and non-avian theropods than in extant birds (Figure 2B).

The power cascade describes bird beak shape within an ecologically informed morphospace

We compared the *Slope* and *Log Aspect Ratio* power cascade parameters of extant bird species to four ecological traits from the literature.[27,40] For this analysis, we only included extant bird species that strongly followed the power cascade ($R^2 \geq$ 0.90; $p < 0.0001$; N = 99, Table S5) and parameters generated from the 3D measurements of the prenarial region in the beak.

When mapping ecological trait categories on the power cascade morphospace, diet (carnivore, herbivore, and omnivore) was the only trait to show apparent group separation (Figure 3A; Figure S7). This division was not evident along the *Slope* axis, with no significant correlation between the *Slope* and diet when accounting for phylogeny ($p > 0.05$, λ = 0.6183, Table S6). The division is evident along the *Log Aspect Ratio* axis, where there was a separation between herbivores and omnivores from the carnivores. The herbivores and omnivores were found to have a more robust beak shape than carnivores, which generally had gracile beaks. This association between diet and the *Log Aspect Ratio* was significant when accounting for a slight phylogenetic signal (p = 0.0125, λ = 0.5256, Table S6). This finding is further supported when assessing if the *Log Aspect Ratio* parameter significantly differed under ecological selective diet regimes when using a multi-optimum Ornstein-Uhlenbeck (OU) evolution analysis.[41] The multi-regime OU model was the best-fitting model for the diet and the *Log Aspect Ratio* (Table S7*)*. Under the multi-regime OU model, the optimal *Log Aspect Ratio* trait estimates for carnivore, omnivore, and herbivore diets ranged from gracile to intermediate to robust-shaped beaks, respectively (Figure 3A; Table S8).

To further explore how adaptation to various diets may affect the evolution of the power cascade parameters, we used a Bayesian state-dependent, relaxed-clock model of Brownian motion evolution (MuSSCRat[42]), implemented in RevBayes.[39] We find the state-dependent model was not supported for the *Log Aspect Ratio* (mean posterior probability of state-dependent model = 0.311 ± 0.003, Figure S8). This implies that diet has no significant influence on the rate of evolution of the *Log Aspect Ratio*. Diet was found to affect the rate of evolution of the *Slope* (Figure 3B, mean posterior probability of the state-dependent model = 0.946 ± 0.008). Omnivores had the highest evolutionary rate for *Slope* (mean = 2.209, 95% HPD = 1.530, 2.704), while rates of *Slope* evolution for herbivores (mean = 0.388, 95% HPD = 0.0979, 0.8102) and carnivores (mean = 0.404, 95% HPD = 0.118, 0.833) overlapped (Figures 3B and 3D). When investigating the background rates of *Slope* evolution (changes in *Slope* not directly related to diet), increased rates of *Slope* evolution were notable early in crown bird evolution, particularly in the Palaeognathae, Anseriformes and Galliformes (Figure S9). An increase in the *Slope* background evolutionary rates was also observed in the Cariamiformes (Red-legged seriema) as well as the ‘‘raptors’’, which include the Accipitriformes and Falconiformes (Figure S9). These groups all had high *Slope* values, including the Eastern osprey, which had the most pointed and convex beak shape.

Diet was found to also affect the rate of evolution for the R^2 value (mean posterior probability of state-dependent model = 0.998 ± 0.0003), which captures how closely an extant bird beak followed the power cascade model (Figure 3C). Omnivores had the highest evolutionary rate (mean = 1.961, 95% HPD = 1.272, 2.576), while herbivores (mean = 0.731, 95% HPD = 0.200, 1.396) and carnivores (mean = 0.308, 95% HPD = 0.128, 0.500) rates overlapped (Figure 3B). When comparing the

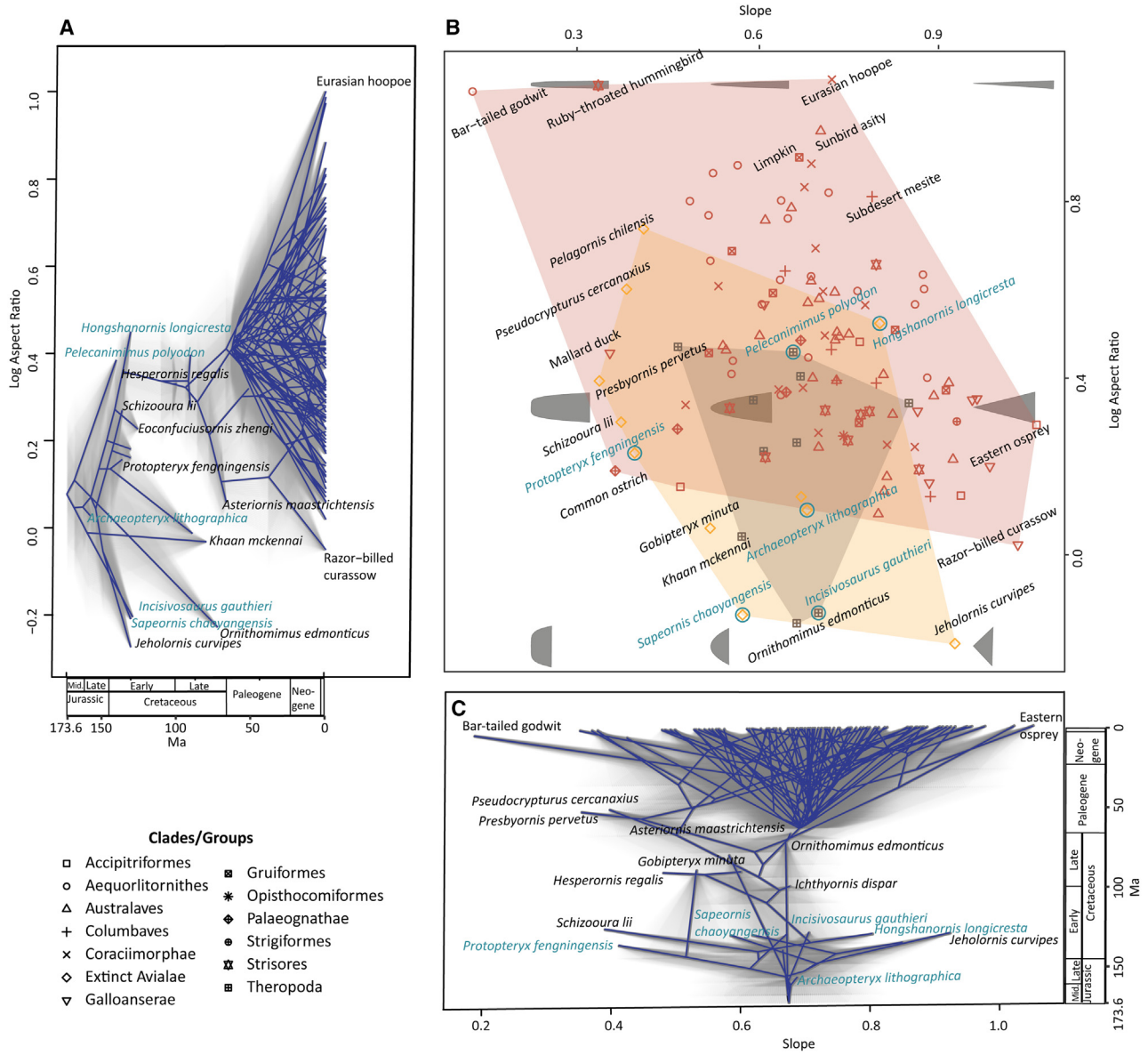

Figure 2. The power cascade describes the diverse shapes of theropod beak and snout evolution

The power cascade parameters (*Slope* and *Log Aspect Ratio*) through evolutionary time.

(A and C). traitgrams show the evolutionary diversification of *Log Aspect Ratio* (A) and *Slope* (C) parameters across the reconstructed phylogeny of theropod taxa that follow the power cascade model ($R^2 > 0.90$). Ancestral state estimation of parameters calculated using maximum likelihood. Gray shading represents a 95% confidence interval. Light blue taxa are those that have teeth on the premaxilla.

(B) The power cascade morphospace using *Slope* and *Log Aspect Ratio* parameters. The *Slope* is the degree of pointedness where a *Slope* of 1 is triangular, and a *Slope* less than 1 is blunter. *Log Aspect Ratio* is the length of the premaxilla divided by the width of the premaxilla base.

background rates (R^2) against state-dependent rates (diet and R^2, Figure S11), an increase in rates of R^2 alone was observed in Pelecaniformes (including the Eurasian spoonbill, Brown pelican and Shoebill, Figures S10 and S11).

Consistent exceptions to the power cascade model of growth

The species that did not follow the power cascade ($R^2 < 0.90$) were similar in both 3D and 2D models and included the Eurasian spoonbill (*Platalea leucorodia*), brown pelican (*Pelecanus occidentalis*), greater painted-snipe (*Rostratula benghalensis)*, and James's flamingo (*Phoenicoparrus jamesi*). The 3D models also captured additional shape information, resulting in the mallard duck (*Anas platyrhynchos*), shoebill (*Balaeniceps rex*), and ruby-throated hummingbird (*Archilochus colubris*) not following the power cascade model in addition to those in the 2D measurements ($R^2 < 0.90$, Table S2).The Ascension frigatebird (*Fregata aquila*) and greater rhea (*Rhea americana*) were the only taxa

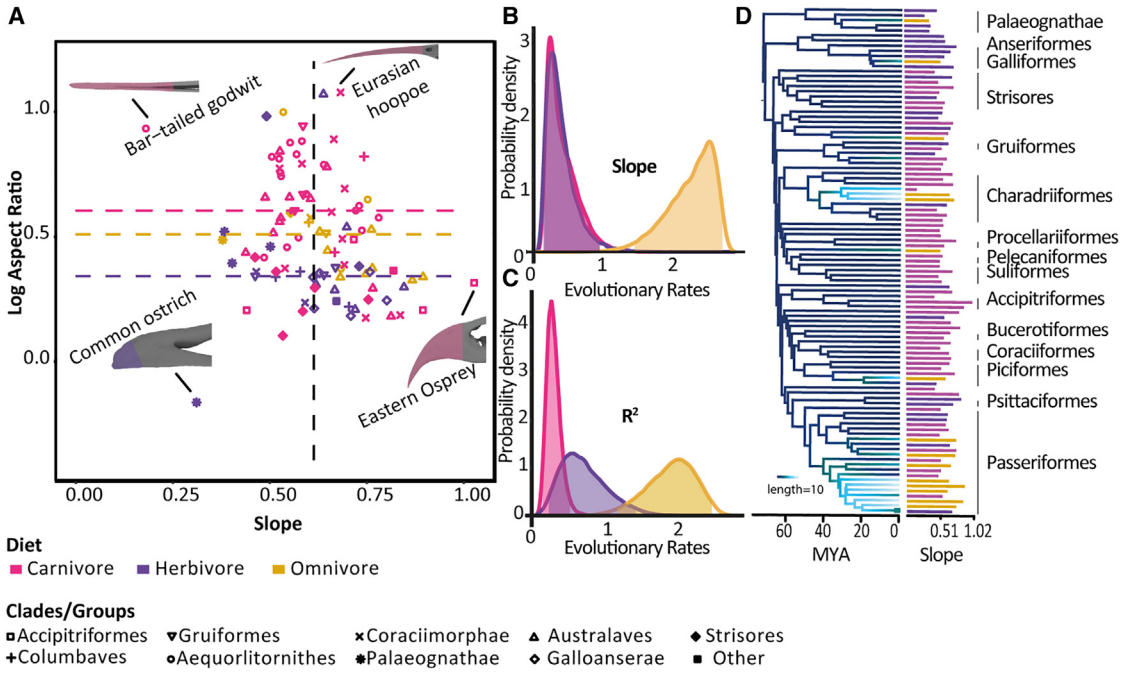

Figure 3. Extant bird beaks show diverse ecological adaptations within the developmental model of growth described by the power cascade

(A) Morphospace of extant bird beaks based on power cascade *Slope* and *Log Aspect Ratio*. 3D beak measurement of the tip of all beaks. A *Slope* value of 1 is a conical shape, and less than 1 is a blunter beak shape. The *Log Aspect Ratio* is the beak length divided by the width of the base. Colors represent the diet: pink—carnivore, purple—herbivore, and yellow—omnivore. Dashed lines represent the estimated optima value from the multi-optimum Ornstein-Uhlenbeck evolutionary analysis. The shape represents Clade/Group. State-dependent rates of (B) *Slope* and (C) R^2 power cascade parameters for each diet category were estimated using the Bayesian, state-dependent, relaxed-clock model of Brownian motion trait evolution.

(D) State-dependent rates of Slope evolution across the extant bird phylogeny with corresponding *Slope* values. Bar colors represent Diet: pink —carnivore, purple—herbivore, and yellow—omnivore. For analysis of *Slope and log Aspect ratio,* only extant bird species that strongly followed the power cascade are included ($R^2 \geq 0.90$; $p < 0.0001$; $N = 99$). For analysis on R^2, all extant birds were included ($n = 106$).

that failed to follow the power cascade in 2D ($R^2 < 0.90$, Table S2).

Beaks were classified as simple or compound in structure, depending on the degree of fusion between the premaxilla body and the subnarial bars.[43] We compared the power cascade model when we measured various beak regions (tip, prenarial, and whole, Figure S2). In bird and extinct theropod beaks classified as simple, the prenarial and whole regions measured in 2D were significantly correlated for *Slope* and *Intercept* ($p < 0.01$; adjusted $R^2 = 1$, Figures S12–S14). We found that the *Intercept* was significantly correlated between all compound beak regions (tip, prenarial, and whole, Figures S12 and S13; Table S9). The *Slope* parameter was significantly correlated between the whole and prenarial regions of the compound beak in 2D (Figures S12 and S13; Table S9). Generally, compound beak shapes deviated more from the power cascade model when prenarial and whole beak areas were measured, compared to the tip (Figure S13).

DISCUSSION

A conserved model of theropod beak and snout shape and growth

Theropods have convergently evolved beaks multiple times, making them an ideal taxon to test if the power cascade model influences the evolution and growth of beak shape. We found that the power cascade model explained a large majority of beak shapes across theropod evolution and the shape of ancestral theropod snouts. Importantly, the snout of a theropod and the beak of crown birds are structurally different. Theropod snouts predominantly comprise the maxilla and premaxilla, while crown bird beaks are almost solely the premaxilla.[14,44] Despite this, the highly derived and structurally different region of bird rostra follows the same power cascade developmental pattern as the non-avian theropod snouts. Therefore, the power cascade model may be a more fundamental growth pattern common among the rostrum of all theropods, and we suggest it may more broadly underpin the growth of all vertebrate rostra. We speculate that this pattern of growth is linked to fundamental and highly conserved rules that describe the growth of the frontonasal region of the skull. Such conserved growth patterns have been suggested to occur in the frontonasal region to stop deleterious morphologies in early development.[44] We, therefore, expect that with more extensive sampling of vertebrate beaks and snouts, the power cascade will remain a predominant pattern of growth and form, while other variations from the power cascade model of growth are also expected to arise. While we may see tinkering of this growth pattern for different ecological adaptations, the underlying power cascade model is substantially influencing observed rostrum shape among vertebrates.

Crown birds have diverse power cascade shapes and growth patterns

With the evolution of crown birds (Neornithes) and diversification after the late end-Cretaceous mass extinction,[45] we observed an increased variance of power cascade beak shapes. Before that time, all theropod taxa investigated had more conserved power cascade beak shapes that were robust and blunt relative to crown birds. Edentulism and the beak evolved from a common ancestor to all Neornithes[9,46] in the Late Cretaceous. When coupled with other evolutionary selective factors,[47] this tooth loss may have enabled the exploration of new variations of power cascade beak shapes. Specifically, more narrow beaks (high aspect ratio) evolved in crown birds, a shape change in theropod beaks that has been attributed previously to the loss of grasping digits on the wings of earlier birds and transition toward pedomorphy in the skull.[21,48] We postulate that this evolution of narrow beaks may also be because the loss of teeth enables beaks with low relative surface area to evolve as they were no longer developmentally constrained to retain space for tooth development.

The increase in power cascade shape diversity in birds may not be linked to increased evolutionary rates. Previous studies have found that within birds, the rostrum showed the fastest evolutionary rates of shape change compared to other skull regions.[49] However, when compared against non-avian theropods, bird rostra and skulls had a slower evolutionary rate.[49] Likewise, we found that the rate of R^2 evolution, or fit to the power cascade, decreased with the evolution of crown birds (Figure S6). This suggests that the overall rate of beak evolution in birds is relatively slow, with the exception of birds that may rapidly evolve along a single branch to a beak shape for specific adaptations, breaking the power cascade.

Ecological adaptation within the developmental model of growth

Extant bird beaks show diverse morphological adaptations that are specialized for ecological niches while following a power cascade growth model. The greatest degree of association between power cascade beak shape changes and functional adaptation was found when coarse-scale ecological levels (i.e., diet: carnivore, herbivore, and omnivore) were considered. At finer ecological levels with more specific dietary types and foraging styles (i.e., trophic niches, number of categories = 24, Figure S7), associated morphological differences in power cascade beak shape were less apparent. This is expected given that the form–function signal in beaks is complex, with a multitude of factors influencing beak shape.[24,50] Perhaps finer ecological levels could be insightful when looking at power cascade parameter beak shape changes at the family level. Such nuanced dietary categorization is also important if the power cascade is used to estimate diet or foraging behavior in extinct theropods.[17,51,52] Nonetheless, the capability of the power cascade model to describe such a diverse range of beak shapes for a multitude of ecological adaptations highlights its universality as a model of beak growth and shape.

The *Aspect Ratio* and *Slope* power cascade parameters differ in their association with diet. When evolving toward herbivory, beaks with a low *Aspect Ratio* were found to be evolutionarily optimal. This is intuitive, given that herbivorous birds have more robust beak shapes, which enable powerful bite forces for processing plant material.[29] In contrast, the evolutionary optimum for carnivore beak shape was a higher *Aspect Ratio*. Carnivorous birds have been found to have more gracile beak shapes for efficiently capturing and processing prey.[24] Generally, the *Aspect Ratio* is well recognized as a main difference in bird beak morphology and has long been related to diet in Galapagos finches[37] and across all birds.[29]

A single selective optimum was identified for all dietary types for the *Slope* parameter. This suggests a broad range of power cascade shapes adapted for different foraging purposes can be generated from a range of *Slope* values. Interestingly, changes in the evolutionary rates of the *Slope* parameter were found to be associated with diet, while the *Aspect Ratio* was not. Compared to carnivores and herbivores, omnivorous birds were found to have significantly higher evolutionary rates of change in *Slope*. This may suggest that a change in the *Slope* value in these omnivorous birds occurred when evolution toward sharpness or bluntness was specifically selected for by their modified omnivorous diet. Indeed, different growth parameters of bird beaks have been suggested to develop and evolve independently.[32]

The diurnal birds of prey, or "raptors", exhibit fast background rates of *Slope* evolution (i.e., increased rates of evolution not directly due to the diet categories) and high associated *Slope* values (Figure S9). This suggests that this group has rapidly evolved pointed beaks due to a selection pressure other than general carnivory. This group is noted for convergently evolving their hooked-shaped beaks that specialize in tearing the flesh of their prey.[24] Raptor beak and skull shape variation did not show species-level variation associated with different carnivorous diets (e.g., carrion, insects, fish).[24] Perhaps including the metric of beak *Slope* or pointedness, in addition to shape measurement of beak curvature and jugal width, could better disentangle fine-scale dietary associations in raptors.

Evolutionary rates of the R^2 value or the fit of beaks to the power cascade model were also associated with diet. Furthermore, the evolution of omnivory in birds was also related to faster evolutionary rates toward lower R^2 values—suggesting that omnivory is associated with increased rates of evolution toward beak shapes that do not follow the power cascade model. This result is contrary to previous reports that omnivory in birds has lower transitionary and diversification rates than other dietary groups.[53] Furthermore, in our study, there were instances in which omnivory evolved and evolutionary rates increased, but these did not result in a change in how well beaks fit the power cascade model. Interestingly, the carnivorous Pelecaniformes was the only clade to have fast background rates of R^2 values (Figures S10 and 11). This suggests that in Pelecaniformes, the selection for a factor other than carnivory has resulted in the rapid shape diversification to beaks that broke the power cascade model. Instead, this finding may result from birds' rapidly evolving beaks that break the power cascade for specialist adaptations, a trait more frequently ascribed to omnivores (e.g., Ruby-throated hummingbird: *Archilochus colubris*) but could also be attributed to the Pelecaniformes in our study (e.g., Eurasian spoonbill: *Platalea leucorodia*). A finer-scale

categorization between omnivores[50,53] and specialists may enable further dissection of our evolutionary rate results.

Overall, birds have evolved diverse ecological adaptations while frequently following the power cascade model in beak shape. The most parsimonious explanation for this phenomenon is that the power cascade describes an underlying developmental or biophysical mechanism for generating a beak. An alternative is that selection for different adaptations coincidentally resulted in birds having beaks that follow the power cascade model. Previous studies have found that bird skull and beak shape diversity occurs within a developmentally defined space.[24,30,34,44] We, therefore, suggest that the power cascade is a developmental mechanism that generates the essential beak shapes that selection acts on to evolve beaks for specific functions.

Additional function and development signals generate exceptions to the power cascade model of growth

Functional pressures may lead to morphological changes that result in beaks not following a power cascade growth model. The types of beaks that failed to follow the power cascade were highly elongated and specialized for unique feeding adaptations, including nectarivory (Ruby-throated hummingbird), aquatic surface filter feeding (Eurasian spoonbill, James's flamingo, and Mallard duck), and plunge diving (Brown pelican). Similarly, previous work has found that nectivores and aquatic foragers have higher rates of beak morphological evolution[29,50] compared to bird species of other trophic classifications. Elongated and highly specialized beaks may or may not follow the power cascade growth model. For instance, while the Ruby-throated hummingbird fails to follow the power cascade model, the confamilial nectarivorous Buff-tailed sicklebill does follow the power cascade model ($R^2 = 0.97$). The morphospace occupation of extant birds shows that the power cascade is a versatile rule of growth that can generate multiple beak shapes. Still, at times, the selection of specific beak shapes to fill a narrow niche space[29] resulted in beaks that deviate from the model. This is further supported by high rates of beak shape evolution occurring at single branches of avialans in this and other studies.[29] These high rates of evolution are significantly associated with increased rates of evolution to low R^2 values and so evolving to break the power cascade model in finding alternative beak shapes.

The degree to which a beak follows the power cascade model of growth may also be related to its proximity to other structures on the cranium. When measuring only the prenarial region of the beak, more species of birds follow the power cascade model than when the entire beak was measured. This may be due to other developmental growth patterns, including the growth of the nares, masking or overriding the power cascade growth pattern. Indeed, we suggest that proximity to other developmental modules (e.g., the more proximal regions of the beak and its juxtaposition to the nares and cranium) increases developmental and shape integration,[25,28,54,55] so overlaying developmental shape patterns are expected. Variations from the power cascade may prove helpful when trying to detect additional developmental processes and function adaptations in regions of the beak.

Conclusion

Previous analyses of beak shape had been unable to describe or predict beak shape and evolution across Theropoda. Here, we find that the power cascade model describes a large majority of theropod beak shapes and rostrum shapes, in general. This growth rule persists with the evolution of beak structures in extant birds adapted to specialized ecological functions. The power cascade, while not unbreakable, is strongly adhered to, pointing to underlying biophysical or developmental mechanisms forming the face of theropods.

Limitations of the study

We strived to capture the immense diversity of theropods by sampling species from 106 out of 253 extant bird families and 42 out of 44 orders. However, it is expected that further sampling of living and extinct theropod rostra will identify additional taxa that follow and deviate from the power cascade rule of growth. Likewise, studying patterns of power cascade shape evolution in light of more fine-scale ecological categories will provide additional nuance.

RESOURCE AVAILABILITY

Lead contact

Further information and requests for resources and data should be directed to and will be fulfilled by the lead contact, Kathleen Garland (kathleen.garland@monash.edu)

Materials availability

This study did not generate new unique reagents.

Data and code availability

- Data micro-CT scans of extant bird bony premaxillae were sourced from either the TEMPO bird project (Morphosource: https://www.morphosource.org/projects/00000C420), KUBI Ornithology Collection (MorphoSource: https://www.morphosource.org/projects/000375320), prior scans (M. Sánchez-Villagra, and T. Green), or scanned from the Museums Victoria, Melbourne, Australia (NMV) collection or the Monash University Zoology Resource Collection (MZRC) (MorphoSource: https://www.morphosource.org/projects/000711879/).
- All original code and associated data sources have been deposited at Monash Bridges in the project titled, "Common Developmental Origins of Beak Shapes and Evolution in Theropods" and are publicly available at the date of publication.
- Any additional information required to reanalyze the data reported in this paper is available from the lead contact upon request.

ACKNOWLEDGMENTS

K.L.S.G. was supported by the Australian Government Research Training Program Scholarship, Monash Graduate Excellence Scholarship, and Robert Blackwood Partnership PhD Top-Up Scholarship. A.R.E. and D.J.F. are supported by Australian Research Council DP230100613. D.J.F. acknowledges additional support from UKRI grant MR/X015130/1.

We would like to thank R. Benson and the TempoBird MorphoSource, as well as the museum collections that provided the CT scans of the extant birds in this project, and T. Green, P. Gignac and M. Sánchez-Villagra for providing additional bird CT scans. For comments and discussion, we would like to thank M. Zelditch, M. McGee, D. Rovinsky, W. Parker, J. Rule, J. Kotevski and J. Abramyan. The authors thank the two reviewers, M. Pittman and P.D. Polly, for their help in revising this paper.

AUTHOR CONTRIBUTIONS

A.R.E. and K.L.S.G. designed the research. K.L.S.G. performed data collection. A.R.E., K.L.S.G., and E.M.H. analyzed data. D.J.F. provided phylogenetic data and advised in phylogenetic analysis and evolutionary interpretation. K.L.S.G., A.R.E., and E.M.H. wrote the paper.

DECLARATION OF INTERESTS

The authors declare no competing interests.

STAR★METHODS

Detailed methods are provided in the online version of this paper and include the following:

- KEY RESOURCES TABLE
- EXPERIMENTAL MODEL AND SUBJECT DETAILS
  - Dataset
- METHOD DETAILS
  - Power cascade shape measurement and analysis
- QUANTIFICATION AND STATISTICAL ANALYSIS
  - Phylogenetic tree assembly
  - Model-based analysis of power cascade fit and parameters
  - Rates of power cascade evolution for theropod beaks and snouts
  - Phylogenetic comparative analysis: Ecological traits

SUPPLEMENTAL INFORMATION

Supplemental information can be found online at https://doi.org/10.1016/j.isci.2025.112246.

Received: December 16, 2024
Revised: February 11, 2025
Accepted: March 14, 2025
Published: March 19, 2025

REFERENCES

1. Thompson, D.W. (1942). On Growth and Form (Cambridge University Press).
2. Kavanagh, K.D., Evans, A.R., and Jernvall, J. (2007). Predicting evolutionary patterns of mammalian teeth from development. Nature *449*, 427–432. https://doi.org/10.1038/nature06153.
3. Smith, J.M., Burian, R., Kauffman, S., Alberch, P., Campbell, J., Goodwin, B., Lande, R., Raup, D., and Wolpert, L. (1985). Developmental constraints and evolution: A perspective from the Mountain Lake Conference on development and evolution. Q. Rev. Biol. *60*, 265–287. https://doi.org/10.1038/nature06153.
4. Newman, S.A. (2015). Development and evolution: The physics connection. In Conceptual change in biology: scientific and philosophical perspectives on evolution and development Boston Studies in the Philosophy and History of Science, A.C. Love, ed. (Springer Netherlands), pp. 421–440. https://doi.org/10.1007/978-94-017-9412-1_19.
5. Raup, D.M. (1966). Geometric analysis of shell coiling: General problems. J. Paleontol. *40*, 1178–1190.
6. Johnson, A.B., Fogel, N.S., and Lambert, J.D. (2019). Growth and morphogenesis of the gastropod shell. Proc. Natl. Acad. Sci. USA *116*, 6878–6883. https://doi.org/10.1073/pnas.1816089116.
7. Evans, A.R., Pollock, T.I., Cleuren, S.G.C., Parker, W.M.G., Richards, H.L., Garland, K.L.S., Fitzgerald, E.M.G., Wilson, T.E., Hocking, D.P., and Adams, J.W. (2021). A universal power law for modelling the growth and form of teeth, claws, horns, thorns, beaks, and shells. BMC Biol. *19*, 58. https://doi.org/10.1186/s12915-021-00990-w.
8. Wynd, B.M., Martínez, R.N., Colombi, C., and Alcober, O. (2020). A review of vertebrate beak morphologies in the triassic: A framework to characterize an enigmatic beak from the Ischigualasto formation, San Juan, Argentina. Ameghiniana *57*, 370–387. https://doi.org/10.5710/AMGH.13.05.2020.3313.
9. Brocklehurst, N., and Field, D.J. (2021). Macroevolutionary dynamics of dentition in Mesozoic birds reveal no long-term selection towards tooth loss. iScience *24*, 102243. https://doi.org/10.1016/j.isci.2021.102243.
10. Davit-Béal, T., Tucker, A.S., and Sire, J.-Y. (2009). Loss of teeth and enamel in tetrapods: fossil record, genetic data and morphological adaptations. J. Anat. *214*, 477–501. https://doi.org/10.1111/j.1469-7580.2009.01060.x.
11. Louchart, A., and Viriot, L. (2011). From snout to beak: The loss of teeth in birds. Trends Ecol. Evol. *26*, 663–673. https://doi.org/10.1016/j.tree.2011.09.004.
12. Meade, L.E., Pittman, M., Balanoff, A., and Lautenschlager, S. (2024). Cranial functional specialisation for strength precedes morphological evolution in Oviraptorosauria. Commun. Biol. *7*, 436–510. https://doi.org/10.1038/s42003-024-06137-1.
13. Miller, C.V., Pittman, M., Kaye, T.G., Wang, X., Bright, J.A., and Zheng, X. (2020). Disassociated rhamphotheca of fossil bird Confuciusornis informs early beak reconstruction, stress regime, and developmental patterns. Commun. Biol. *3*, 519–526. https://doi.org/10.1038/s42003-020-01252-1.
14. O'Connor, P.M., Turner, A.H., Groenke, J.R., Felice, R.N., Rogers, R.R., Krause, D.W., and Rahantarisoa, L.J. (2020). Late Cretaceous bird from Madagascar reveals unique development of beaks. Nature *588*, 272–276. https://doi.org/10.1038/s41586-020-2945-x.
15. Hu, H., Wang, Y., McDonald, P.G., Wroe, S., O'Connor, J.K., Bjarnason, A., Bevitt, J.J., Yin, X., Zheng, X., Zhou, Z., and Benson, R.B.J. (2022). Earliest evidence for fruit consumption and potential seed dispersal by birds. Elife *11*, e74751. https://doi.org/10.7554/eLife.74751.
16. Ma, W., Pittman, M., Butler, R.J., and Lautenschlager, S. (2022). Macroevolutionary trends in theropod dinosaur feeding mechanics. Curr. Biol. *32*, 677–686.e3. https://doi.org/10.1016/j.cub.2021.11.060.
17. Miller, C.V., and Pittman, M. (2021). The diet of early birds based on modern and fossil evidence and a new framework for its reconstruction. Biol. Rev. *96*, 2058–2112. https://doi.org/10.1111/brv.12743.
18. Wang, S., Stiegler, J., Wu, P., Chuong, C.-M., Hu, D., Balanoff, A., Zhou, Y., and Xu, X. (2017). Heterochronic truncation of odontogenesis in theropod dinosaurs provides insight into the macroevolution of avian beaks. Proc. Natl. Acad. Sci. USA *114*, 10930–10935. https://doi.org/10.1073/pnas.1708023114.
19. Bhullar, B.A.S., Hanson, M., Fabbri, M., Pritchard, A., Bever, G.S., and Hoffman, E. (2016). How to make a bird skull: Major transitions in the evolution of the avian cranium, paedomorphosis, and the beak as a surrogate hand. Integr. Comp. Biol. *56*, 389–403. https://doi.org/10.1093/icb/icw069.
20. Wang, S., Stiegler, J., Wu, P., and Chuong, C.-M. (2020). Tooth versus beak: The evolutionary developmental control of the avian feeding apparatus in Pennaraptoran theropod dinosaurs: Past progress and new frontiers. Bull. Am. Mus. Nat. Hist. *440*, 205–228.
21. Bhullar, B.-A.S., Marugán-Lobón, J., Racimo, F., Bever, G.S., Rowe, T.B., Norell, M.A., and Abzhanov, A. (2012). Birds have paedomorphic dinosaur skulls. Nature *487*, 223–226.
22. Yang, T.-R., and Sander, P.M. (2018). The origin of the bird's beak: new insights from dinosaur incubation periods. Biol. Lett. *14*, 20180090. https://doi.org/10.1098/rsbl.2018.0090.
23. Plateau, O., and Foth, C. (2020). Birds have peramorphic skulls, too: anatomical network analyses reveal oppositional heterochronies in avian skull evolution. Commun. Biol. *3*, 195–212. https://doi.org/10.1038/s42003-020-0914-4.
24. Bright, J.A., Marugán-Lobón, J., Cobb, S.N., and Rayfield, E.J. (2016). The shapes of bird beaks are highly controlled by nondietary factors. Proc.

Natl. Acad. Sci. USA *113*, 5352–5357. https://doi.org/10.1073/pnas.1602683113.

25. Felice, R.N., and Goswami, A. (2018). Developmental origins of mosaic evolution in the avian cranium. Proc. Natl. Acad. Sci. USA *115*, 555–560. https://doi.org/10.1073/pnas.1716437115.
26. Navalón, G., Bright, J., Marugán-Lobón, J., and Rayfield, E. (2018). The evolutionary relationship between beak shape, mechanical advantage, and feeding ecology in modern birds. Evolution *73*, 422–435. https://doi.org/10.1111/evo.13655.
27. Pigot, A.L., Sheard, C., Miller, E.T., Bregman, T.P., Freeman, B.G., Roll, U., Seddon, N., Trisos, C.H., Weeks, B.C., and Tobias, J.A. (2020). Macroevolutionary convergence connects morphological form to ecological function in birds. Nat. Ecol. Evol. *4*, 230–239. https://doi.org/10.1038/s41559-019-1070-4.
28. Navalón, G., Marugán-Lobón, J., Bright, J.A., Cooney, C.R., and Rayfield, E.J. (2020). The consequences of craniofacial integration for the adaptive radiations of Darwin's finches and Hawaiian honeycreepers. Nat. Ecol. Evol. *4*, 270–278. https://doi.org/10.1038/s41559-019-1092-y.
29. Cooney, C.R., Bright, J.A., Capp, E.J.R., Chira, A.M., Hughes, E.C., Moody, C.J.A., Nouri, L.O., Varley, Z.K., and Thomas, G.H. (2017). Mega-evolutionary dynamics of the adaptive radiation of birds. Nature *542*, 344–347. https://doi.org/10.1038/nature21074.
30. Young, N.M., Linde-Medina, M., Fondon, J.W., Hallgrímsson, B., and Marcucio, R.S. (2017). Craniofacial diversification in the domestic pigeon and the evolution of the avian skull. Nat. Ecol. Evol. *1*, 95–98. https://doi.org/10.1038/s41559-017-0095.
31. Campàs, O., Mallarino, R., Herrel, A., Abzhanov, A., and Brenner, M.P. (2010). Scaling and shear transformations capture beak shape variation in Darwin's finches. Proc. Natl. Acad. Sci. USA *107*, 3356–3360. https://doi.org/10.1073/pnas.0911575107.
32. Mallarino, R., Grant, P.R., Grant, B.R., Herrel, A., Kuo, W.P., and Abzhanov, A. (2011). Two developmental modules establish 3D beak-shape variation in Darwin's finches. Proc. Natl. Acad. Sci. USA *108*, 4057–4062. https://doi.org/10.1073/pnas.1011480108.
33. Rands, C.M., Darling, A., Fujita, M., Kong, L., Webster, M.T., Clabaut, C., Emes, R.D., Heger, A., Meader, S., Hawkins, M.B., et al. (2013). Insights into the evolution of Darwin's finches from comparative analysis of the Geospiza magnirostris genome sequence. BMC Genom. *14*, 95. https://doi.org/10.1186/1471-2164-14-95.
34. Fritz, J.A., Brancale, J., Tokita, M., Burns, K.J., Hawkins, M.B., Abzhanov, A., and Brenner, M.P. (2014). Shared developmental programme strongly constrains beak shape diversity in songbirds. Nat. Commun. *5*, 3700. https://doi.org/10.1038/ncomms4700.
35. Al-Mosleh, S., Choi, G.P.T., Abzhanov, A., and Mahadevan, L. (2021). Geometry and dynamics link form, function, and evolution of finch beaks. Proc. Natl. Acad. Sci. USA *118*, e2105957118. https://doi.org/10.1073/pnas.2105957118.
36. Rubin, C.-J., Enbody, E.D., Dobreva, M.P., Abzhanov, A., Davis, B.W., Lamichhaney, S., Pettersson, M., Sendell-Price, A.T., Sprehn, C.G., Valle, C.A., et al. (2022). Rapid adaptive radiation of Darwin's finches depends on ancestral genetic modules. Sci. Adv. *8*, eabm5982. https://doi.org/10.1126/sciadv.abm5982.
37. Mosleh, S., Choi, G.P.T., Musser, G.M., James, H.F., Abzhanov, A., and Mahadevan, L. (2023). Beak morphometry and morphogenesis across avian radiations. Proc. Biol. Sci. *290*, 20230420. https://doi.org/10.1098/rspb.2023.0420.
38. Boucher, F.C., and Démery, V. (2016). Inferring bounded evolution in phenotypic characters from phylogenetic comparative data. Syst. Biol. *65*, 651–661. https://doi.org/10.1093/sysbio/syw015.
39. Höhna, S., Landis, M.J., Heath, T.A., Boussau, B., Lartillot, N., Moore, B.R., Huelsenbeck, J.P., and Ronquist, F. (2016). RevBayes: Bayesian phylogenetic inference using graphical models and an interactive model-specification language. Syst. Biol. *65*, 726–736. https://doi.org/10.1093/sysbio/syw021.
40. Tobias, J.A., Sheard, C., Pigot, A.L., Devenish, A.J.M., Yang, J., Sayol, F., Neate-Clegg, M.H.C., Alioravainen, N., Weeks, T.L., Barber, R.A., et al. (2022). AVONET: Morphological, ecological and geographical data for all birds. Ecol. Lett. *25*, 581–597. https://doi.org/10.1111/ele.13898.
41. Cressler, C.E., Butler, M.A., and King, A.A. (2015). Detecting adaptive evolution in phylogenetic comparative analysis using the Ornstein–Uhlenbeck model. Syst. Biol. *64*, 953–968. https://doi.org/10.1093/sysbio/syv043.
42. May, M.R., and Moore, B.R. (2020). A Bayesian approach for inferring the impact of a discrete character on rates of continuous-character evolution in the presence of background-rate variation. Syst. Biol. *69*, 530–544. https://doi.org/10.1093/sysbio/syz069.
43. Hieronymus, T.L., and Witmer, L.M. (2010). Homology and evolution of avian compound rhamphothecae. Auk *127*, 590–604. https://doi.org/10.1525/auk.2010.09122.
44. Young, N.M., Hu, D., Lainoff, A.J., Smith, F.J., Diaz, R., Tucker, A.S., Trainor, P.A., Schneider, R.A., Hallgrímsson, B., and Marcucio, R.S. (2014). Embryonic bauplans and the developmental origins of facial diversity and constraint. Development *141*, 1059–1063. https://doi.org/10.1242/dev.099994.
45. Brusatte, S.L., O'Connor, J.K., and Jarvis, E.D. (2015). The Origin and Diversification of Birds. Curr. Biol. *25*, R888–R898. https://doi.org/10.1016/j.cub.2015.08.003.
46. Meredith, R.W., Zhang, G., Gilbert, M.T.P., Jarvis, E.D., and Springer, M.S. (2014). Evidence for a single loss of mineralized teeth in the common avian ancestor. Science *346*, 1254390. https://doi.org/10.1126/science.1254390.
47. Larson, D.W., Brown, C.M., and Evans, D.C. (2016). Dental Disparity and Ecological Stability in Bird-like Dinosaurs prior to the End-Cretaceous Mass Extinction. Curr. Biol. *26*, 1325–1333. https://doi.org/10.1016/j.cub.2016.03.039.
48. Bhullar, B.-A.S., Morris, Z.S., Sefton, E.M., Tok, A., Tokita, M., Namkoong, B., Camacho, J., Burnham, D.A., and Abzhanov, A. (2015). A molecular mechanism for the origin of a key evolutionary innovation, the bird beak and palate, revealed by an integrative approach to major transitions in vertebrate history. Evolution *69*, 1665–1677. https://doi.org/10.1111/evo.12684.
49. Felice, R.N., Watanabe, A., Cuff, A.R., Hanson, M., Bhullar, B.-A.S., Rayfield, E.R., Witmer, L.M., Norell, M.A., and Goswami, A. (2020). Decelerated dinosaur skull evolution with the origin of birds. PLoS Biol. *18*, e3000801. https://doi.org/10.1371/journal.pbio.3000801.
50. Felice, R.N., Tobias, J.A., Pigot, A.L., and Goswami, A. (2019). Dietary niche and the evolution of cranial morphology in birds. Proc. Biol. Sci. *286*, 20182677. https://doi.org/10.1098/rspb.2018.2677.
51. Miller, C.V., Bright, J.A., Wang, X., Zheng, X., and Pittman, M. (2024). Synthetic analysis of trophic diversity and evolution in Enantiornithes with new insights from Bohaiornithidae. Elife *12*, RP89871. https://doi.org/10.7554/eLife.89871.
52. Miller, C.V., Pittman, M., Wang, X., Zheng, X., and Bright, J.A. (2022). Diet of Mesozoic toothed birds (Longipterygidae) inferred from quantitative analysis of extant avian diet proxies. BMC Biol. *20*, 101. https://doi.org/10.1186/s12915-022-01294-3.
53. Burin, G., Kissling, W.D., Guimarães, P.R., Şekercioğlu, Ç.H., and Quental, T.B. (2016). Omnivory in birds is a macroevolutionary sink. Nat. Commun. *7*, 11250. https://doi.org/10.1038/ncomms11250.
54. Kulemeyer, C., Asbahr, K., Gunz, P., Frahnert, S., and Bairlein, F. (2009). Functional morphology and integration of corvid skulls – a 3D geometric morphometric approach. Front. Zool. *6*, 2. https://doi.org/10.1186/1742-9994-6-2.
55. Orkney, A., Bjarnason, A., Tronrud, B.C., and Benson, R.B.J. (2021). Patterns of skeletal integration in birds reveal that adaptation of element shapes enables coordinated evolution between anatomical modules.

Nat. Ecol. Evol. *5*, 1250–1258. https://doi.org/10.1038/s41559-021-01509-w.

56. Paradis, E., and Schliep, K. (2019). ape 5.0: An environment for modern phylogenetics and evolutionary analyses in R. Bioinformatics *35*, 526–528. https://doi.org/10.1093/bioinformatics/bty633.
57. Castiglione, S., Tesone, G., Piccolo, M., Melchionna, M., Mondanaro, A., Serio, C., Di Febbraro, M., and Raia, P. (2018). A new method for testing evolutionary rate variation and shifts in phenotypic evolution. Methods Ecol. Evol. *9*, 974–983. https://doi.org/10.1111/2041-210X.12954.
58. Revell, L.J. (2012). phytools: An R package for phylogenetic comparative biology (and other things). Methods Ecol. Evol. *3*, 217–223. https://doi.org/10.1111/j.2041-210X.2011.00169.x.
59. Pinheiro, J., and Bates, D. (1999). nlme: Linear and Nonlinear Mixed Effects Models. R package version *3*, 1–166. https://doi.org/10.32614/CRAN.package.nlme.
60. Pennell, M.W., Eastman, J.M., Slater, G.J., Brown, J.W., Uyeda, J.C., FitzJohn, R.G., Alfaro, M.E., and Harmon, L.J. (2014). geiger v2.0: An expanded suite of methods for fitting macroevolutionary models to phylogenetic trees. Bioinformatics *30*, 2216–2218. https://doi.org/10.1093/bioinformatics/btu181.
61. Beaulieu, J.M., Jhwueng, D.-C., Boettiger, C., and O'Meara, B.C. (2012). Modeling stabilizing selection: Expanding the Ornstein-Uhlenbeck model of adaptive evolution. Evolution *66*, 2369–2383. https://doi.org/10.1111/j.1558-5646.2012.01619.x.
62. Bjarnason, A., and Benson, R. (2021). A 3D geometric morphometric dataset quantifying skeletal variation in birds. MorphoMuseuM *7*, e125. https://doi.org/10.18563/journal.m3.125.
63. Stange, M., Núñez-León, D., Sánchez-Villagra, M.R., Jensen, P., and Wilson, L.A.B. (2018). Morphological variation under domestication: how variable are chickens? R. Soc. Open Sci. *5*, 180993. https://doi.org/10.1098/rsos.180993.
64. Green, T.L., and Gignac, P.M. (2021). Osteological description of casque ontogeny in the southern cassowary (Casuarius casuarius) using micro-CT imaging. Anat. Rec. *304*, 461–479. https://doi.org/10.1002/ar.24477.
65. Gill, F., Donsker, D., and Rasmussen, P. (2023). IOC World Bird List. https://doi.org/10.14344/IOC.ML.13.1.
66. Field, D.J., Benito, J., Chen, A., Jagt, J.W.M., and Ksepka, D.T. (2020). Late Cretaceous neornithine from Europe illuminates the origins of crown birds. Nature *579*, 397–401. https://doi.org/10.1038/s41586-020-2096-0.
67. Wang, M., and Zhou, Z. (2019). A new confuciusornithid (Aves: Pygostylia) from the Early Cretaceous increases the morphological disparity of the Confuciusornithidae. Zool. J. Linn. Soc. *185*, 417–430. https://doi.org/10.1093/zoolinnean/zly045.
68. Zhou, Z., and Zhang, F. (2005). Discovery of an ornithurine bird and its implication for Early Cretaceous avian radiation. Proc. Natl. Acad. Sci. USA *102*, 18998–19002. https://doi.org/10.1073/pnas.0507106102.
69. Field, D.J., Hanson, M., Burnham, D., Wilson, L.E., Super, K., Ehret, D., Ebersole, J.A., and Bhullar, B.-A.S. (2018). Complete Ichthyornis skull illuminates mosaic assembly of the avian head. Nature *557*, 96–100. https://doi.org/10.1038/s41586-018-0053-y.
70. Balanoff, A.M., Xu, X., Kobayashi, Y., Matsufune, Y., and Norell, M.A. (2009). Cranial Osteology of the Theropod Dinosaur Incisivosaurus gauthieri (Theropoda: Oviraptorosauria). Am. Mus. Novit. *3651*, 1–35. https://doi.org/10.1206/644.1.
71. Balanoff, A.M., and Norell, M.A. (2012). Osteology of Khaan mckennai (Oviraptorosauria: Theropoda). Bull. Am. Mus. Nat. Hist. *372*, 1–77. https://doi.org/10.1206/803.1.
72. Zhou, Z., and Zhang, F. (2006). A beaked basal ornithurine bird (Aves, Ornithurae) from the Lower Cretaceous of China. Zool. Scr. *35*, 363–373. https://doi.org/10.1111/j.1463-6409.2006.00234.x.
73. Chiappe, L.M., Norell, M., and Clark, J. (2001). A New Skull of Gobipteryx minuta (Aves: Enantiornithes) from the Cretaceous of the Gobi Desert. Am. Mus. Novit. *3346*, 1–15. https://doi.org/10.1206/0003-0082(2001)346<0001:ANSOGM>2.0.CO;2.
74. Shuang, Z., Zhong-He, Z., and O'connor, J. (2012). A new basal beaked ornithurine bird from the lower cretaceous of western Liaoning, China. Vert. PalAs. *50*, 9.
75. Bell, A., and Chiappe, L.M. (2020). Anatomy of Parahesperornis: Evolutionary Mosaicism in the Cretaceous Hesperornithiformes (Aves). Life *10*, 62. https://doi.org/10.3390/life10050062.
76. Lefèvre, U., Hu, D., Escuillié, F., Dyke, G., and Godefroit, P. (2014). A new long-tailed basal bird from the Lower Cretaceous of north-eastern China. Biol. J. Linn. *113*, 790–804. https://doi.org/10.1111/bij.12343.
77. Norell, M.A., Makovicky, P.J., and Currie, P.J. (2001). Palaeontology. The beaks of ostrich dinosaurs. Nature *412*, 873–874. https://doi.org/10.1038/35091139.
78. Choiniere, J.N., Forster, C.A., and de Klerk, W.J. (2012). New information on *Nqwebasaurus thwazi*, a coelurosaurian theropod from the Early Cretaceous Kirkwood Formation in South Africa. J. Afr. Earth Sci. *71–72*, 1–17. https://doi.org/10.1016/j.jafrearsci.2012.05.005.
79. Zhang, F., Zhou, Z., and Benton, M.J. (2008). A primitive confuciusornithid bird from China and its implications for early avian flight. Sci. China Ser. D-Earth. Sci. *51*, 625–639. https://doi.org/10.1007/s11430-008-0050-3.
80. Schwarz, D., Kundrát, M., Tischlinger, H., Dyke, G., and Carney, R.M. (2019). Ultraviolet light illuminates the avian nature of the Berlin Archaeopteryx skeleton. Sci. Rep. *9*, 6518. https://doi.org/10.1038/s41598-019-42823-5.
81. Nesbitt, S.J., and Clarke, J.A. (2016). The Anatomy and Taxonomy of the Exquisitely Preserved Green River Formation (Early Eocene) Lithornithids (Aves) and the Relationships of Lithornithidae. Bull. Am. Mus. Nat. Hist. *406*, 1–91. https://doi.org/10.1206/0003-0090-406.1.1.
82. Hu, H., O'Connor, J.K., McDonald, P.G., and Wroe, S. (2020). Cranial osteology of the Early Cretaceous *Sapeornis chaoyangensis* (Aves: Pygostylia). Cretac. Res. *113*, 104496. https://doi.org/10.1016/j.cretres.2020.104496.
83. Mayr, G., and Rubilar-Rogers, D. (2010). Osteology of a new giant bony-toothed bird from the Miocene of Chile, with a revision of the taxonomy of Neogene Pelagornithidae. J. Vertebr. Paleontol. *30*, 1313–1330. https://doi.org/10.1080/02724634.2010.501465.
84. Chiappe, L.M., Di, L., Serrano, F.J., Yuguang, Z., and Meng, Q. (2020). Anatomy and Flight Performance of the Early Enantiornithine Bird Protopteryx fengningensis: Information from New Specimens of the Early Cretaceous Huajiying Formation of China. Anat. Rec. *303*, 716–731. https://doi.org/10.1002/ar.24322.
85. R Core Team (2013). R: A Language and Environment for Statistical Computing (Foundation for Statistical Computing) Version 4.4.1. .
86. Prum, R.O., Berv, J.S., Dornburg, A., Field, D.J., Townsend, J.P., Lemmon, E.M., and Lemmon, A.R. (2015). A comprehensive phylogeny of birds (Aves) using targeted next-generation DNA sequencing. Nature *526*, 569–573. https://doi.org/10.1038/nature15697.
87. Ding, A., Pittman, M., Upchurch, P., O'Connor, J., Field, D.J., and Xu, X. (2020). The Biogeography of Coelurosaurian theropods and its impact on their evolutionary history. Bull. Am. Mus. Nat. Hist. *40*, 117–157.
88. Landis, M.J., and Schraiber, J.G. (2017). Pulsed evolution shaped modern vertebrate body sizes. Proc. Natl. Acad. Sci. USA *114*, 13224–13229. https://doi.org/10.1073/pnas.1710920114.
89. Eastman, J.M., Alfaro, M.E., Joyce, P., Hipp, A.L., and Harmon, L.J. (2011). A novel comparative method for identifying shifts in the rate of character evolution on trees. Evolution *65*, 3578–3589. https://doi.org/10.1111/j.1558-5646.2011.01401.x.
90. Revell, L.J., and Harmon, L.J. (2022). Phylogenetic Comparative Methods in R (Princeton University Press).

STAR★METHODS

KEY RESOURCES TABLE

REAGENT or RESOURCE	SOURCE	IDENTIFIER
Deposited Data		
3D CT- and surface scans of 103 extant bird species TEMPO bird project Benson	https://www.morphosource.org/projects/00000C420	See Table S1 for the complete specimen list.
3D CT- and surface scans of Gallus gallus,PIMUZ_159; *Casuarius casuarius*, TLGC 0010	Collaborators (M.S.V and T.L.G)	See Table S1 for specimen information.
3D CT- and surface scans of Rhea american (NMVB.23639) and Dromaius novaehollandiae (MZRC6163). Theropod Premaxilla Power Cascade: Additional Bird Skulls	https://www.morphosource.org/projects/000711879/	See Table S1 for specimen information.
Surface scan of Aegotheles insignis (KUO:113304) Beyond the beak: brain size and allometry in avian craniofacial evolution. Benson	https://www.morphosource.org/projects/000375320	See Table S1 for specimen information.
2D fossil images	Various published literature.	See Table S1 for specimen information.
Image Attributions for Figure 1	Image silhouettes are from PhyloPic https://www.phylopic.org; Keesey, 2023	Contributions are as follows: ● Yellow-throated toucan by Federico Degrange (2019; CC0 1.0) ● Red-fan parrot by Myriam Ramirez (2019; CC0 1.0); ● Bar-Tailed godwit by Andy Wilson (2024; CC0 1.0); ● Common sunbird-asity by Campbell Fleming (2020; CC0 1.0) ● Silver Gull by Marie-Aimée Allard (2023; CC0 1.0) ● *Archaeopteryx* by T. Michael Keesey (2011; CC0 1.0) ● Emu by Darren Naish (vectorize by T. Michael Keesey) (2014; CC0 1.0) ● *Incisivosaurus* modified by illustration by Tom Parker (2013;CC0 1.0).
Extant bird trophic niche and habitat data.	AVONET[40]	figshare: [https://doi.org/10.26180/28457168] See Table S5.
Extant bird foraging niche data.	Pigot et al.[27]	https://doi.org/10.1038/s41559-01910704.
R-code and associated data	figshare: [https://doi.org/10.26180/28457168]	Monash Bridges Platform
RevBayes script	figshare: [https://doi.org/10.26180/28510283]	Monash Bridges Platform
Software and algorithms		
Avizo	Thermo Fisher Scientific	https://www.thermofisher.com
Geomagic Wrap	3D systems	https://www.3dsystems.com
Rhinoceros v. 5/6	Robert McNeel & Associates	https://www.rhino3d.com
RevBayes	Höhna et al.[39]	https://revbayes.github.io/
MuSSCRat	May and Moore[42]	https://github.com/mikeryanmay/musscrat_supp_archive

(*Continued on next page*)

Continued

REAGENT or RESOURCE	SOURCE	IDENTIFIER
R Studio v4.2.1(reference)	R Core Team	https://www.r-project.org
ape (R package)	Paradis et al.[56]	https://cran.r-project.org/web/packages/ape/index.html
RRphylo (R package)	Castiglione et al.[57]	https://cran.r-project.org/web/packages/RRphylo/index.html
Phytools (R package)	Revell[58]	https://cran.r-project.org/web/packages/phytools/index.html
faux (R package)	DeBruine(2020)	https://cran.r-project.org/web/packages/faux/index.html
nlme (R package)	Pinheiro et al.[59]	https://cran.r-project.org/web/packages/nlme/index.html
geiger (R package)	Pennel et al.[60]	https://cran.r-project.org/web/packages/geiger/index.html
OUwie (R package)	Beaulieu[61]	https://cran.r-project.org/web/packages/OUwie/index.html
RevGadgets (R package)	Höhna et al.[39]	https://cran.r-project.org/web/packages/RevGadgets/index.html

EXPERIMENTAL MODEL AND SUBJECT DETAILS

Dataset

3D measurements of extant bird beaks were made from micro-CT scans. A total of 106 micro-CT scans of extant bird bony premaxillae were sourced from either the TEMPO bird project(Morphosource),[62] KUBI Ornithology Collection (MorphoSource), prior scans (Sanchez,[63] and Green[64]), or scanned from the collections of Museums Victoria, Melbourne, Australia (NMV). See Table S1 for more information. These micro-CT scans covered 106 extant bird species from 106 families spanning the avian phylogeny (106 out of 253 families and 42 out of 44 orders).[65] Micro-CT scans were processed in Avizo (version 2022.1). We removed all keratin surrounding the premaxilla using automatic and manual thresholding and segmentation techniques to ensure the premaxilla and not the keratinous rhinotheca were measured. The models were then smoothed, and foramina filled in Geomagic Wrap (version 2015).

The 3D models were used to collect 2D measurements of extant bird beaks. To measure fossil specimens in 2D, we sourced 21 theropod fossil specimens with beaks and snouts from previous publications. These specimens and publications they were sourced from is as follows, *Asteriornis maastrichtensis* (NHMM 2013 008)[66]; *Confuciusornis sanctus* (IVPP V12352)[67]; *Hongshanornis longicresta* (IVPP V14533)[68]; *Ichthyornis dispar* (ALMNH 3316)[69]; *Incisivosaurus gauthieri* (IVPPV 13326)[70]; *Khaan mckennai* (IGM 100/973)[71]*; Archaeorhynchus spathula* (IVPP V14287)[72]*; Gobipteryx minuta (ZPAL-MgRI32)*[73]*; Schizooura lii* (IVPP V 16761)[74]; *Hesperornis regalis* (KUVP 71012)[75]; *Parahesperornisae alexi (KUVP 2287)*[75]; *Jeholornis curvipes* (YFGP yb2)[76]; *Ornithomimus edmonticus* (RTMP 95.110.1)[77]; *Pelecanimimus polyodon* (LH7777)[78]; *Eoconfuciusornis zhengi* (IVPP V11977)[79]; *Archaeopteryx lithographica* (MB.Av.101)[80]; *Pseudocrypturus cercanaxius* (USNM 336103)[81]; *Sapeornis chaoyangensis* (IVPP V19058)[82]; *Presbyornis pervetus* (USNM 299846)[66]; *Pelagornis chilensis (*MNHN SGO.PV 1061)[83]; *Protopteryx fengningensis* (BMNHC Ph 1060)[84] (Table S1).

METHOD DETAILS

Power cascade shape measurement and analysis

To assess whether a beak followed the power cascade model, two sets of measurements were made: distance measurements along the midline of the structure and associated average radius measurements. Power cascade measurements were made following previously established methods[7] and carried out Rhinoceros 3D v. 5.0 or 6.0 (Robert McNeel & Associates, Seattle, WA, USA), as described briefly below.

For 3D models, we calculated the midline.[7] Along this midline, we placed 20 equidistant points. At each point, we measured the 3D cross-sectional area perpendicular to the midline. The radius was calculated from this value (Radius= $\sqrt{}$ [cross-sectional area/π]).

2D models were measured by tracing the beak outline in a lateral plane, excluding teeth if present. As with 3D models, 20 equidistance points were placed along the midline. The diameter of the outline perpendicular to the midline was measured at these points. The radius was then calculated (Radius=Diameter/2). To reduce invariability, it is important that cross-sections/diameters are made at 90° from the midline in both 2D and 3D.

Beaks were defined as simple or compound, depending on the degree of fusion between the premaxilla body and the subnarial bars.[43] Prenarial and tip regions of the beaks in 2D and 3D were made only in the region of premaxilla that was fused as a single

bony element. See graphic methods (Figure S2) to describe how different regions of simple and compound beaks were measured in 3D and 2D.

A single person (KLSG) made all power cascade measurements to remove inter-observer error. All statistical analysis was completed in R[85] unless otherwise stated.

QUANTIFICATION AND STATISTICAL ANALYSIS

Phylogenetic tree assembly

To create our composite time-scaled phylogeny of the theropod taxa measured in this study, we use the function bind.tree in 'ape'[56] and tree.merger in 'RRpylo'[57] to combine published phylogenies. When species were not present in the phylogeny, a cogener or other sister taxon with similar divergence time was used (i.e. *Jeholornis curvipes*: *Jeholornis prima*, *Pseudocrypturus cercanaxius*: *Paracathartes howardae*, *Pelecanimimus polyodon*: *Nqwebasaurus thwazi)*. We sourced topologies and divergence dates from recent literature.[9,29,86,87] For extant birds, the backbone of the phylogeny was sourced from Prum et al.,[86] with more densely sampled patch clades from Brocklehurst and Field.[9]

Model-based analysis of power cascade fit and parameters

We fit an unbounded Brownian Motion model, bounded Brownian motion[38] and an Ornstein-Uhlenbeck evolutionary model to assess which model best explains the evolution of beak shapes in relation to how well they fit the power cascade model of shape and growth. The trait value (R^2) can vary within the set bounds of 0 and 1 in this model. This model was compared to unbounded Brownian motion and an Ornstein-Uhlenbeck evolutionary model with AICc. This analysis was done using the *bounded_bm* function in 'phytools'. To map the R^2 values onto the theropod phylogeny, we used *ancr* on the bounded Brownian model and *contMap* in 'phytools'.[58]

For those theropod taxa that strongly follow the power cascade model of shape and growth ($R^2 > 0.90$), we modelled the evolution of the *Slope* and L*og Aspect Ratio* parameters using the function *fastAnc* and *fancyTree* in 'phytools'.[88] These functions construct ancestral states along a phylogeny using maximum likelihood analysis with 95% confidence intervals.

Rates of power cascade evolution for theropod beaks and snouts

To assess how the rate of evolution for power cascade-shaped beaks and snouts (R^2) changed over the theropod phylogeny, we conducted continuous relaxed Brownian motion models to see the branch-specific rates of R^2 evolution.[89] Transformed R^2 values from the ancestral state estimation were used to meet the assumptions of the *Gaussian* model.[88] R^2 was transformed using the *unif2norm* function in 'faux' where μ and standard deviation were set to 0 and 1, accordingly. A square root transformation was then applied to the values as the data was negatively skewed. Transformed R^2 values were found to be normally distributed using the Shapiro-Wilk test ($W = 0.98$, p-value = 0.104). Relaxed Brownian motion models were conducted in RevBayes version 1.2.4[39] (supplementary RevBayes script). The MCMC was run for 50,000 generations, with a burn-in of 10%. Tracer (version 1.7.2) was used to visualise log files and verify convergence of the MCMC by ensuring ESS values were above 200 for all key parameters. Because priors can influence the analysis outcomes, we repeated RevBayes models using three different priors on the number of evolutionary rate shifts (1, 5, and 10 rate shifts). Priors had little influence on model output therefore, we present the results of the default model when following the RevBayes tutorial, with five rate shifts.

Phylogenetic comparative analysis: Ecological traits

We were interested in the association between the power cascade parameters and the various ecological and behavioural adaptations in extant birds. Consequently, we sourced ecological factors that previous studies found correlated with beak shape. All traits were categorical and included diet (trophic level, category number=3), trophic niche (category number=10), and habitat (category number=9), which were sourced from AVONET (33), as well as foraging niche (category number=24), which was sourced from Pigot et al.[27] See Table S5 for a summary of traits. Due to some groups being represented by two or fewer species, phylogenetic analysis was not conducted for the foraging niche and habitat category. All phylogenetic comparative analyses for *Slope,* and *Log Aspect Ratio* were undertaken only on those extant bird taxa with premaxilla shapes that followed the power cascade model of growth ($R^2 > 0.90$; $p < 0.0001$; $N = 99$).

First, we used a phylogenetic Generalized Least Squares Analysis (PGLS) to test if there was a correlation between the power cascade parameters (*Slope* and *Log Aspect Ratio*) and various ecological factors (diet, foraging, foraging niche, and habitat). The PGLS was performed using the 'ape'[56] and 'nlme' packages.[59] The phylogenetic signal (λ) parameter was used to account for the phylogenetic effect.

To further explore how the power cascade parameters, vary with ecological and behavioural adaptations in extant birds, we conducted a multi-optimum Ornstein-Uhlenbeck evolution analysis. When comparing the different transitional rates models (i.e., equal-rates, symmetric, and all-rates different), the best-described regime shift across the phylogeny for diet was the all-rates-different using the AICc criterion, while for Trophic Niche and Habitat, it was the Equal-Rates Model (52, Table S10). Models were created using the *fitDiscrete* function in 'geiger'.[60]

Using the *make.simmap* function in 'phytools',[58] we mapped the best-fit models for diet and foraging transitions onto the extant bird phylogeny. These stochastic maps were then used with the *OUwie* function in 'OUwie'[61] to model trait-related regime shifts for

Slope and *Log Aspect Ratio* parameters. We hypothesised that birds with different diets should have different regimes of natural selection acting upon them, causing species of similar diets to have more similar *Log Aspect Ratio* and *Slope* parameters. To test this hypothesis, we compared the fit of (1) a single-rate Brownian motion model, (2) a model in which the rate of evolution may vary, and (3) an Ornstein-Uhlenbeck model with a single optimum for all species, (4) a multi-regime OU model. In the multi-regime OU model, the rate of stochastic evolution (σ^2) and the strength of directed evolution toward the optima (α) may vary.[90] The *OUwie* function can only use a single stochastic map generated from a single permutation. We ensured this single stochastic map corresponded with the regime shifts generated from the consensus simulation map from 1000 permutations.

We tested the influence of trophic level on the evolution of *Slope, Log Aspect Ratio,* and R^2 using a Bayesian approach by modelling multiple state-specific rates of continuous character evolution (MuSSCRat).[42] The MuSSCRat model enables us to test how the discrete variable of trophic level directly influences the evolution of the continuous characters of *Slope*, *Log Aspect Ratio,* and R^2 separately under a Brownian motion model of evolution. These models are advantageous because they also consider the influence of background rate variation, which is variation in rates of the continuous character not directly due to the evolution of the discrete characters of interest. All MuSSCRat analyses were conducted in RevBayes version 1.2.4[39] (supplementary RevBayes script). The MCMC was run for 500,000 generations, with a burn-in of 10%. Tracer (version 1.7.2) was used to visualise log files and verify convergence of the MCMC by ensuring ESS values were above 200 for all key parameters. Because priors can influence the outcomes of analyses, we repeated RevBayes models using three different priors on the number of rate shifts (1, 5, and 10 rate shifts). Priors had little influence on model output (Supplementary RevBayes Output); therefore, we present the results of the default model when following the RevBayes tutorial with five rate shifts.